

Solar Heating of a Stratified Ocean in the Presence of a Static Ice Cover

DONALD K. PEROVICH

U.S. Army Cold Regions Research and Engineering Laboratory, Hanover, New Hampshire

GARY A. MAYKUT

Department of Atmospheric Sciences, University of Washington, Seattle

Conductivity, temperature, and depth measurements were carried out in an isolated transverse lead in static, shorefast ice in Mould Bay, Prince Patrick Island, Northwest Territories, during a 3-week period at the height of the melt season. Currents beneath the ice appeared to be weak and largely tidal in nature. Initially, the water was vertically uniform and at the salinity-determined freezing point down to a depth of at least 20 m. By the end of the experiment the water column consisted of three distinct layers: a well-mixed, nearly fresh surface meltwater layer; a very stable half-meter-thick halocline centered somewhat below the bottom of the ice; and a thermally stratified layer of constant salinity extending down to at least 25 m. The halocline was characterized by a temperature maximum that was about 2°C warmer than the surrounding water. This temperature maximum in the pycnocline effectively trapped shortwave energy absorbed in the lower layer and prevented it from melting the overlying ice. Theoretical calculations demonstrate that the thermal structure observed beneath the pycnocline was controlled by the input of shortwave radiation and that vertical heat transport was largely the result of diffusive processes. The presence of leads drastically increases the amount of energy stored in the water. In regions where leads are common, it is likely that this energy will significantly accelerate the decay and removal of the ice once it becomes mobile and once the pycnocline is erased.

INTRODUCTION

The summer decay of ice in the polar oceans is driven largely by incoming shortwave radiation (F_r). Even in near-shore regions of the Arctic where advection of warm air from nearby land masses can result in substantial turbulent heat exchange over the ice, net radiation still accounts for at least 75% of the total heat input at the surface. Numerous experimental and theoretical studies have been carried out to investigate the role of F_r in the heat and mass balance of a sea ice cover [e.g., Untersteiner, 1961; Langleben, 1966; Maykut and Untersteiner, 1971] and to examine radiative transfer within the ice itself [Maykut and Grenfell, 1975; Grenfell and Maykut, 1977; Perovich and Grenfell, 1981; Grenfell, 1983].

While the direct effects of F_r on the surface and interior of an ice floe are now well understood and fairly easy to treat in models, relatively little is known about the input of F_r to the upper ocean or about its subsequent interaction with the ice cover. Nevertheless, it is clear that solar heating of the water can have a major impact on the state of the ice and the upper ocean. In the southern ocean, for example, where surface ablation is minimal during the summer [Andreas and Ackley, 1982], heat release from the water is the primary factor controlling the seasonal disappearance of the ice cover. It appears that only about 50% of this energy could be derived from water below the pycnocline [Gordon, 1981], indicating that most of the remaining energy must come from shortwave radiation deposited in the upper ocean. In the central Arctic Ocean, physical evidence [Aagaard *et al.*, 1981] and theoretical calculations [Maykut, 1982] both suggest that the magnitude of the oceanic heat flux at the bottom of the ice is

determined almost completely by solar radiation transmitted through the ice pack, rather than by the influx of warm Atlantic water through Fram Strait. Without solar heating of the ocean the thermodynamic equilibrium thickness of ice in the central Arctic would be 2–3 times the present value of 3 m.

Although shortwave radiation transmitted through areas of thin ice and melt ponds can contribute significantly to solar heating of the water column, the amount is usually small compared to the energy (I_w) which enters the ocean through open leads. An open lead absorbs over 90% of F_r , with more than 50% being deposited below the bottom of the ice. Because of the positive feedback between decreasing ice concentration and increasing solar input to the water, considerable attention has been given to the effect of I_w on lateral melting at lead edges. Early theoretical treatments [Zubov, 1945; Langleben, 1972] assumed that all of I_w goes immediately to lateral melting. These models predict an extremely rapid disappearance of the ice cover once the concentration drops below about 70%. Maykut and Perovich [1987], however, argue that only a fraction of I_w can go directly to lateral melting, with other portions contributing to bottom ablation, heat storage in the water column, and losses to the atmosphere. In particular, relative motion between the ice and the underlying water causes radiation absorbed below the bottom of the lead to be advected laterally beneath the surrounding ice where vertical mixing subsequently transports much of this energy to the underside of the ice, where it is lost to bottom ablation. As the ice thins, the portion of I_w that is used for bottom ablation increases, resulting in a positive feedback between ice thickness and vertical heat transport to the bottom of the ice which is almost as effective at removing ice as the feedback between ice concentration and lateral melting [Maykut and Perovich, 1987]. Seasonal decay patterns are thus sensitive

Copyright 1990 by the American Geophysical Union.

Paper number 90JC01117.
0148-0227/90/90JC-01117\$05.00

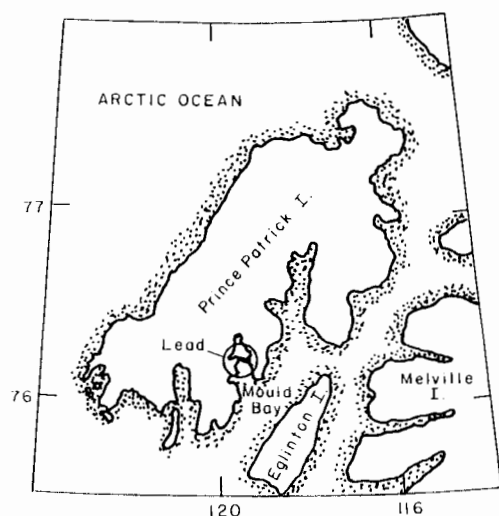


Fig. 1. Prince Patrick Island and environment.

to assumptions regarding the disposition of I_w within the ice-ocean system. For example, model calculations taking into account solar heating of the underlying water predict that seasonal ice should normally disappear as a result of thinning, whereas the Zubov/Langleben approach removes the ice cover primarily by lateral melting, i.e., ice concentration approaches zero while ice thickness remains finite.

Simulations of ice decay in near-shore regions of the Arctic [Maykut and Perovich, 1987] indicate that radiation-induced bottom melting should account for about 25% of the summer mass loss. While few experimental data are available which can be used to verify this estimate, there is observational evidence which appears to suggest that it could be much too large. Measurements made by Langleben [1966] in static first-year ice at Tanquary Fiord on Ellesmere Island during the early part of the melt season (May 14 to June 18) showed 110 cm of surface ablation and no bottom ablation (or accretion). Water temperatures 1 m below the ice increased from -1.4° to -0.4°C during this period, indicating the presence of low-salinity meltwater immediately beneath the ice. Detailed measurements could not be continued once the ice became mobile, but subsequent melting was observed to be extremely rapid, and the ice cover vanished within a matter of days. A possible explanation for the absence of bottom melting, even though substantial amounts of shortwave radiation must have entered the water, is that temperatures remained cold in the lower part of the ice, allowing the conductive flux in the ice (F_c) to balance the oceanic heat flux (F_w) at the bottom of the ice. This, however, does not seem like a realistic explanation. Not only would F_c have been decreasing throughout the melt period while F_w was increasing, but also crude calculations suggest that the ice should have become essentially isothermal long before the end of the observational period. A more plausible explanation is that meltwater runoff stabilized the upper part of the water column and inhibited the upward transport of heat to the ice. In the following sections we present experimental evidence to support this view. We first show details of how the absorption of shortwave radiation and meltwater runoff interact to determine the thermohaline structure of the underlying water, then carry out simple model calculations to quantify effects of I_w on heat storage in

the water, and finally explore potential implications of the phenomenon in the Arctic.

FIELD PROGRAM

During the summer (June 8 to July 13) of 1982 we carried out a field experiment to obtain quantitative information on how shortwave radiation deposited in leads influences the decay of a sea ice cover. We were particularly interested in determining horizontal heat transfer rates to the lead walls and in resolving how I_w was apportioned between lateral and bottom melting. Observations were carried out in the static, shorefast ice of Mould Bay ($76^\circ30'\text{N}$, 119°W), on the south side of Prince Patrick Island in the Canadian Archipelago (Figure 1). The bay was covered by first-year ice which was 2.2 m thick at the beginning of the ablation season; average snow depth was about 0.3 m. Several narrow flaw leads, with an average spacing of about 3–4 km, ran transversely across the entire width of the bay. The lead closest to the Mould Bay weather station was selected for the study. The primary measurement site was located about 1 km from the west shore and 5 km from the east shore, in water that was about 250 m deep [Holt and Digby, 1985]. Figure 2 shows the evolution of this lead from a 2-m-wide snow-filled crack on June 8 to an 11-m-wide, open lead on July 13.

Vigorous surface melting began on June 21, and by June 25 the snow cover was completely gone from the ice and the surrounding land. Many small streams of fresh water were observed to be flowing into the bay from the land during this period of intense snow melting. Immediately after the snow-melt was completed, the surface of the ice was almost completely covered by meltwater. Much of this water drained off within 2–3 days, leaving a surface composed predominantly (60–70%) of shallow ponds (or water-saturated blue ice) interspersed with patches of higher-albedo, drained white ice. Dives beneath the ice indicated that the underside was essentially flat and featureless. By July 13 the surrounding ice had decreased to 1.4 m in thickness, with no evidence of preferential thinning in the vicinity of the lead. Lateral ablation in the lead during this period totaled 1.5 m, although the lead itself widened by 9 m. The reason for this additional widening is not immediately evident. There was no discernible ice movement along the shore, and the increase in lead width was gradual and continuous throughout the experimental period (Figure 3). A possible explanation is that thermal contraction of the ice occurred as it warmed. Thermal expansion coefficients reported by Doronin and Kheisin [1977] are consistent with this view and would produce about 1.5 m more opening than was actually observed. However, Cox [1983] argues that thermal expansion in saline ice should be equal to that for pure ice, in which case the lead should have closed slightly. Thus it is unclear whether the additional widening resulted from thermal contraction of the ice cover or from another mechanism, such as wind-driven differential north-south deformations.

Profiles of temperature and salinity were measured in the lead at 1- to 3-day intervals with Sea-Bird SBE-3 and SBE-4 temperature and conductivity sensors. Vertical profile data were obtained at 0.1-m intervals between the surface and a depth of 1 m, at 0.2-m intervals between 1 and 5 m, and at 1-m intervals between 5 and 25 m. Accurate depth control in the upper 5 m was achieved by attaching the sensors to a



Fig. 2a

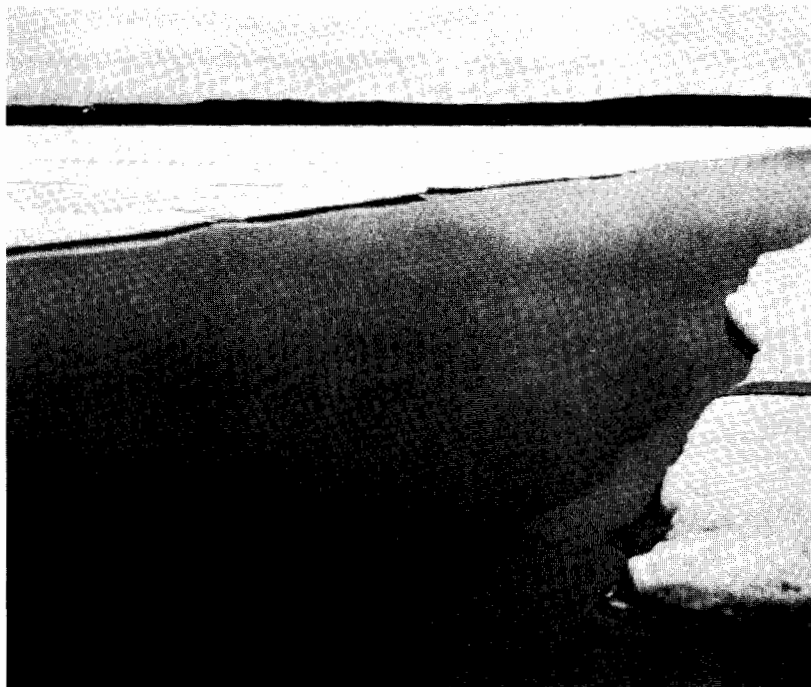


Fig. 2b

Fig. 2. Photographs illustrating the evolution of the lead from (a) a narrow snow-filled crack on June 17 to (b) a 10-m-wide lead on July 10 (12).

rigid pipe which was then lowered into the lead; for depths greater than 5 m the sensor pair was simply attached to the end of a thin cable. Algorithms from *Culkin and Smith* [1980] and *Lewis* [1980] were used to convert conductivities to

salinities, while densities were calculated using an empirical relationship derived by *Gebhart and Mollendorf* [1977]. Absolute accuracies were of the order of 0.01°C and 0.01‰ , or better; however, derived quantities such as heat content

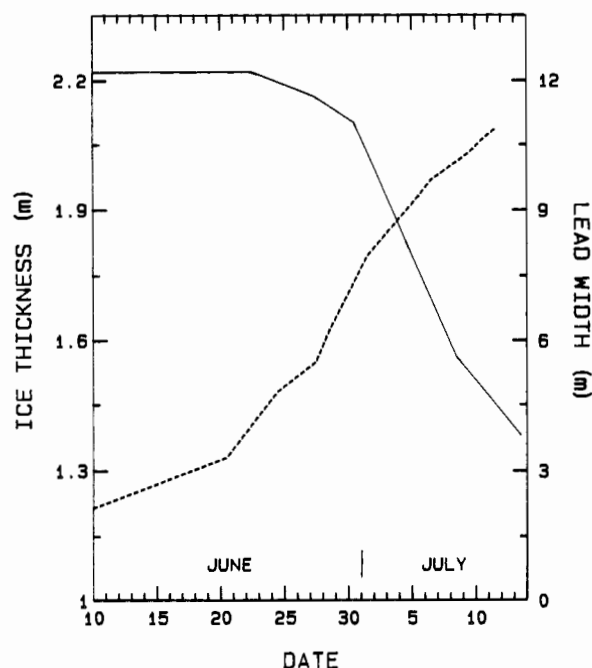


Fig. 3. Observed changes in ice thickness (solid curve) and lead width (dashed curve) during the experimental period.

and stability appeared somewhat noisy when the salinity gradient was steep. This is probably because the salinity values represent a vertical average over 0.1–0.2 m, while temperatures more closely reflect the actual value at a specific depth. Lowering of the sensors may have also produced some local disturbance in the density field.

Most of the conductivity, temperature, and depth (CTD) measurements were taken adjacent to the south wall of the

lead. Although the experiment was not designed to monitor lateral changes in water structure below the ice, horizontal temperature and salinity profiles were occasionally taken at several depths between the surface of the lead and the bottom of the ice. These data revealed that horizontal variations in the lead were generally quite small, and they demonstrate that a single vertical profile is normally sufficient to characterize the temperature and salinity structure of narrow leads. Such may not be the case in larger leads with widths of the order of 100 m or more or in the underlying water column.

Energy fluxes over the ice and lead were calculated from routine meteorological observations (incoming shortwave and long-wave radiation, cloud cover, air temperature, and wind speed) taken at the nearby Mould Bay Weather Station. Environmental conditions and heat balance components for the lead are summarized in Table 1. Although the incident radiation, cloudiness, and wind speed were essentially the same at the weather station and at the lead site, station temperatures were found to be somewhat warmer than those measured at the lead and were reduced accordingly in Table 1. The results show that shortwave radiation was the primary energy source for the lead, averaging 275 W/m^2 during the observational period. Energy gains from the turbulent fluxes (48 W/m^2) and net long-wave radiation losses (43 W/m^2) roughly balanced one another. Approximately one quarter of the total energy deposited in the lead was expended in lateral melting, leaving a sizable remainder for warming of the water and/or melting at the underside of the ice.

THERMOHALINE EVOLUTION OF THE WATER COLUMN

A complete description of the heat and mass balance of the ice and lead has been given by *Perovich* [1983]. Here we

TABLE 1. Summary of Environmental Conditions and Energy Fluxes for the Mould Bay Lead

Date	Lead Width, m	Ice Thickness, m	Surface Temperature, °C	Air Temperature, °C	Wind Speed, m/s	Cloud Cover*	Incident Short-wave, W/m^2	Sensible Heat, W/m^2	Latent Heat, W/m^2	Out-going Long Wave, W/m^2	Incoming Long Wave, W/m^2	Net Heat Flux,† W/m^2	Transmitted Through Ice, W/m^2
June 20	1.3	2.22	-0.67	0.3	4.5	8	310	10	1	-319	285	272	
June 21	2.2	2.22		0.3	4.4	4	316	8	-1	-320	259	246	
June 22	3.1	2.22		1.9	4.4	1	357	22	10	-321	260	310	
June 23	4.0			2.1	4.8	2	352	24	12	-322	262	310	
June 24	4.8		-0.07	2.5	5.7	8	209	31	16	-322	294	218	
June 25				2.5	4.6	8	199	26	14	-322	294	201	
June 26				2.5	5.8	10	178	33	17	-322	321	218	
June 27	5.5	2.16	-0.02	1.7	5.1	7	353	20	8	-322	281	322	
June 28	6.2		0.29	2.5	3.2	6	235	16	8	-324	277	200	8.3
June 29				3.5	8.4	0	332	58	35	-324	266	350	11.5
June 30		2.10		4.0	7.1	2	326	54	35	-325	269	343	11.5
July 1	8.0		0.83	3.0	4.5	7	231	22	11	-326	286	212	9.2
July 2				3.5	4.3	1	338	27	16	-326	266	304	13.8
July 3				3.5	6.1	6	228	40	24	-325	281	237	10.5
July 4		1.83		3.5	2.1	9	126	14	9	-325	310	128	6.4
July 5	9.3		0.40	3.0	3.1	9	170	18	10	-324	309	175	9.3
July 6	9.7		0.27	3.0	6.6	6	241	41	23	-323	279	249	13.8
July 7				5.0	5.2	4	313	55	40	-324	277	345	17.7
July 8		1.56		3.5	6.1	1	335	43	26	-324	266	329	21.3
July 9	10.3		0.46	3.5	6.2	1	312	43	26	-324	266	307	20.7
July 10	10.6		0.44	3.5	5.3	4	312	40	25	-323	271	309	20.5
Average	6.3	2.04	0.21	2.8	5.1	5	275	31	17	-323	280	266	13.4

*Cloud cover is given in tenths.

†The net flux was calculated assuming an albedo of 0.05 for the lead.

would like to focus instead on how the structure and thermal regime of the water beneath the lead responded to the input of meltwater and solar radiation. Temporal changes in the temperature, salinity, and density of the upper 5 m of the water column are summarized in Figure 4. As can be seen from the close correspondence of the salinity and density curves, water density is dominated by salinity effects with temperature having only a small influence. On June 20 (Figure 4a), shortly before the onset of the melt season, the lead was cold, salty, and at its salinity-determined freezing point. The slight amount of freshening evident in the upper half meter was the result of the melting of snow that had drifted into the lead. With the onset of surface melting, there was a rapid influx of fresh water to the lead, and by June 28 (Figure 4b) the water from the surface of the lead to the bottom of the ice had become relatively fresh (3‰), a few tenths of a degree above its freezing point. Below this fresh layer there was a sharp transition to colder (-1.4°C) and saltier (32‰) water. As the ice melt continued, the freshwater layer deepened and by July 6 (Figure 4c) extended about 0.5 m beneath the bottom of the ice. The water column then consisted of three distinct layers: (1) a 2-m-thick, well-mixed, fresh surface layer; (2) a $\frac{1}{2}$ -m-thick, strongly stable halocline; and (3) a slightly stable, 32‰ layer extending down to at least 25 m. The warmest temperatures ($+0.8^{\circ}\text{C}$) were located in the halocline. The water column exhibited the same characteristic three-layer structure on July 10 (Figure 4d) when the last set of CTD measurements was taken. During the July 6–10 period there was a general warming of the entire water column above 12 m (Figure 5). The warming was most pronounced in the halocline where a distinctive bulge in the temperature profile developed with maximum temperatures approaching $+2^{\circ}\text{C}$. There was no significant deepening of the freshwater layer despite continued ice melt. The sharpness of the freshwater/saltwater boundary throughout the melt season indicates that vertical mixing between the two water masses was minimal, although slightly increased salinity between 1.8 and 2.2 m during the July 6–10 period suggests that some vertical diffusion was occurring. This salinity increase appears to have been sufficient to confine new meltwater above 1.8 m, as evidenced by a salinity decrease of about 0.6‰ in the lead.

The heat content of the water column (referenced to the local freezing point) is shown in Figure 6a as a function of depth on June 28, July 6, and July 10; the corresponding heating rates are given in Figure 6b. While there was essentially no heat in the upper 25 m of the water column on June 20, measurable heat had accumulated at all depths by June 28. Below about 3 m the decrease in heat content with depth was roughly exponential, suggesting that the source of the heat was shortwave radiation. Heat buildup in the upper layer was small because of substantial energy losses to the lead walls and ice bottom. Despite a decrease in the average incident shortwave radiation from 279 W/m^2 to 248 W/m^2 , the heating rate below the halocline increased from June 28 to July 6 as the lead widened and the ice thinned. During the final 4 days, F_r increased to 303 W/m^2 , and heating rates above 10 m increased dramatically, more than doubling at the 2- to 3-m level. At the same time, energy absorption below 10 m decreased significantly. The apparent reason for this was increasing biological activity which altered the optical properties of the water. A decrease in the clarity of the water first became evident in late June, after which time

the water was found to be noticeably more murky on each succeeding visit to the lead. The increasing opacity of the water appears to have been the result of a vigorous algal bloom which by July 6 was sufficiently dense to cause nearly complete absorption of transmitted solar energy in the upper 10 m of the water column. The magnitude and shape of the temperature bulge below the halocline must, in part, reflect the presence of these algae; however, the situation was complicated by changes in the state of the ice cover, lead width, and density structure. These factors will be considered in more detail in the following sections.

DISCUSSION

To the best of our knowledge a thermohaline structure of the type observed beneath the ice in Mould Bay has not been previously documented in the polar oceans. Nevertheless, temperature increases of the order of $0.5^{\circ}\text{--}1^{\circ}\text{C}$ appear to be fairly common in water near the bottom of rapidly melting sea ice, both in the near-shore regions [Langleben, 1966] and in the central Arctic (A. Hanson, personal communication, 1975). It has generally been assumed that these elevated temperatures are due to the intrusion of lower-salinity meltwater beneath the ice, rather than to any actual increase in heat content. However, salinity data are lacking in the previous observations, and some degree of solar heating cannot be ruled out. While radiation-induced temperature maxima are known to exist near the surface of large, quiescent leads [Buzuyev and Fedorov, 1973] and in a pair of high-salinity Antarctic lakes [Hoare et al., 1964; Hoare, 1966], the closest analog to the Mould Bay situation occurs in certain ice-covered, freshwater lakes where similar temperature maxima have been observed by Hutchinson [1957] and by Wiegand and Carmack [1981], among others. Hutchinson reports that such features are most commonly found in hard water lakes with relatively opaque water. The high mineral content of the water provides a stabilizing density gradient, while the opacity enhances the absorption of shortwave radiation, resulting in greater warming.

While it seems evident that the temperature bulge and distinct three-layer structure observed beneath the Mould Bay lead resulted from the input of solar heat and meltwater to the water column, other factors also contributed to its maintenance and evolution. Particularly important was the lack of ice movement and the weak water circulation which inhibited mechanical mixing between the lower-density meltwater and the underlying salt water. Concurrent measurements carried out through leads in the mobile ice pack about 5 km north of the island [Perovich, 1983] indicated no such stratification of the meltwater below the bottom of the ice. Much lower ice concentrations in the mobile pack allowed greater amounts of shortwave radiation to enter the water column, and significant warming was observed between July 3 and July 12 (Figure 7). Despite the tendency for solar heating to stabilize seawater, the heat content remained relatively constant down to a depth of 10–15 m, presumably the result of mechanically induced vertical mixing. We conclude that the halocline observed at Mould Bay is a relatively fragile feature which can be maintained only in the absence of strong relative motions between the ice and the water.

Several mechanisms contributed to keeping the fresh surface layer above the halocline well mixed. Primary among

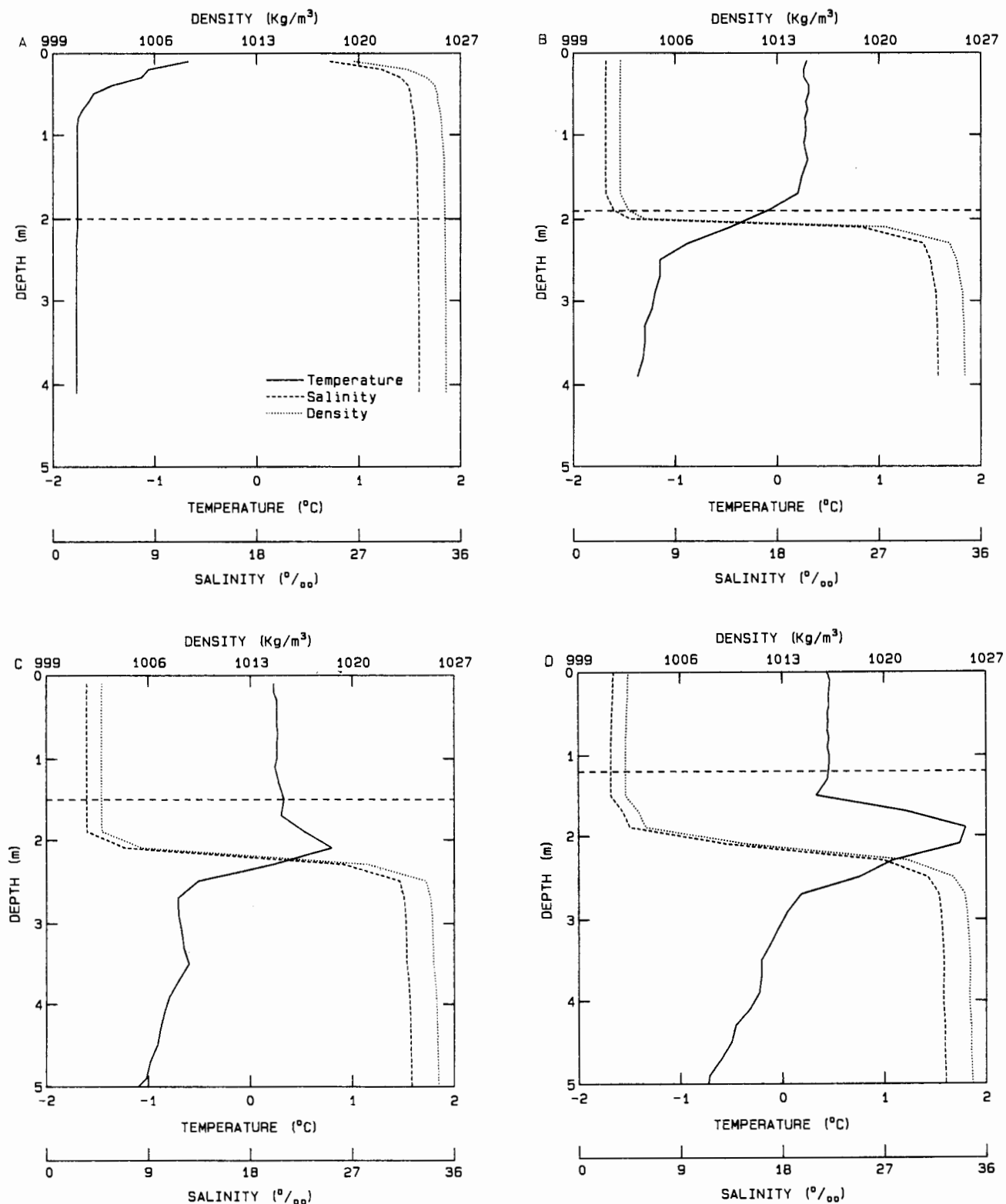


Fig. 4. Vertical profiles of temperature (solid curve), salinity (dashed curve), and density (dotted curve) measured in the upper part of the lead on (a) June 20, (b) June 28, (c) July 6, and (d) July 10. The horizontal dashed line indicates the approximate position of the ice bottom.

these was solar heating. With an average salinity of only 3‰ the temperature of maximum density in the surface layer was 3.4°C. Since upper layer temperatures were always below 3.4°C, the exponentially decreasing input of shortwave energy with depth tended to produce warmer and denser water

near the surface, resulting in negative stability and vertical mixing. The thermally induced density differences, however, were inadequate to overcome those induced by salinity differences, and the vertical mixing did not penetrate the halocline. Dye experiments showed that the wind also made

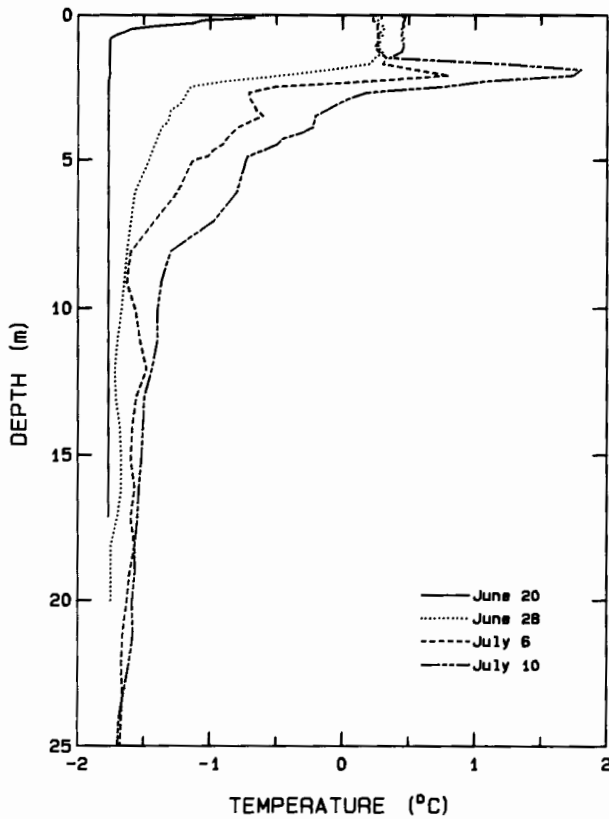


Fig. 5. Evolution of temperature in the upper 25 m of the water column observed beneath the south wall of the lead.

a substantial contribution to mixing in the lead when speeds exceeded a few meters per second, but this mixing was not sufficiently energetic to overcome the strong stability of the halocline and was largely confined to the upper 1–2 m of the water column. Entry of runoff streams from the surrounding land produced surface currents of the order of a few knots in the lead and also contributed to mixing during the early part of the melt season. Because of these processes and the heat sinks provided by the lead edges and ice bottom, heat buildup in the surface layer was minimal, and water temperatures remained near the freezing point throughout the experiment.

In contrast to the low-salinity surface layer, solar heating of water whose salinity exceeds 24.7‰ causes increased stability because warming produces a decrease in density. Thus most of the radiative energy absorbed in the lower part of the halocline and underlying water would tend to remain in place unless disturbed by mechanical mixing. Of course, heat can still be transported vertically by conduction, but such fluxes are usually small compared to those produced by convection. Heat should therefore accumulate with time at all levels below the halocline. Near the top of the halocline there can, depending on the magnitude of the salinity and temperature gradients, be some convection and entrainment by the surface layer. Entrainment in the present case, however, was small because of the steepness of the salinity gradient. Under these conditions it is reasonable to expect that solar heating would lead to the development of a temperature maximum in the halocline. Energy absorbed above the maximum would be conducted upward into the surface layer, while energy absorbed below the maximum

would be slowly conducted downward and trapped in much the same way as in a solar pond. The data shown in Figures 4–6 are consistent with this view.

MODEL SIMULATIONS

Qualitatively, at least, an explanation of the Mould Bay observations appears to be relatively straightforward. It is not clear, however, whether the observed temperature field is in quantitative agreement with the incident radiation fluxes and changing ice conditions. In addition, there are a number of interesting questions which cannot be directly answered with the available data. For example, what was the lateral extent of the temperature maximum, and how did it vary with distance from the lead? To what degree did biological activity and horizontal advection influence the observed profiles? What happened in the water column during the remainder of the summer? To answer such questions with confidence would require time- and depth-dependent data on the current velocity, optical properties of the water, and horizontal distribution of salinity and temperature beneath the ice. Unfortunately, the observational program, being focused on the ice and lead, was not designed to produce such information. Nevertheless, some insights can be gained from the present data set when used in conjunction with simple models of the ice and water.

A Simple Thermo-optical Model

Let us first examine the heat buildup in the water. If we consider only the stable part of the water column (i.e., below the surface layer) and ignore for the moment horizontal variations, then temperature profiles can be calculated using a simple one-dimensional heat conduction equation which includes a source term to describe solar heating at each level:

$$\partial T_w / \partial t = a_z \partial^2 T_w / \partial z^2 + [1/(\rho_w c_w)] dF(z, t)/dz \quad (1)$$

where T_w is the temperature of the water, $a_z = 1.4 \times 10^{-7} \text{ m}^2/\text{s}$ is the molecular diffusivity of the water, $\rho_w = 1000 \text{ kg/m}^3$ is the density of the water, $c_w = 4.185 \text{ kJ/(kg } ^\circ\text{C)}$ is the specific heat of the water, and $F(z, t)$ is the net downwelling irradiance at depth z (below the surface of the lead) and time t . If we subdivide z - t space into subintervals of lengths Δz and Δt , respectively, then (1) may be expressed in a purely implicit, central difference form as

$$(1/\Delta t + 2a_z/\Delta z^2)T_w(i, n+1) - (a_z/\Delta z^2)[T_w(i-1, n+1) + T_w(i+1, n+1)] = T_w(i, n)/\Delta t + \Delta F(i, n+1)/(\rho_w c_w \Delta z) \quad (2)$$

where i is the depth index and n is the time index. Equation (2) represents a system of linear equations which may be solved simultaneously for temperature at each level, given the initial temperature distribution and boundary value changes. The advantage of the implicit formulation is that it is unconditionally stable. In the simulations reported below, we chose $\Delta z = 0.2 \text{ m}$ and $\Delta t = 1 \text{ day}$. The upper boundary was taken to be at the bottom of the surface mixed layer ($z = 1.5 \text{ m}$); the lower boundary was assumed to be at $z = 9.1 \text{ m}$, primarily to achieve sufficient spatial resolution of the temperature maximum while keeping the size of the solution matrix manageable.

The most difficult part of the calculation is the estimation

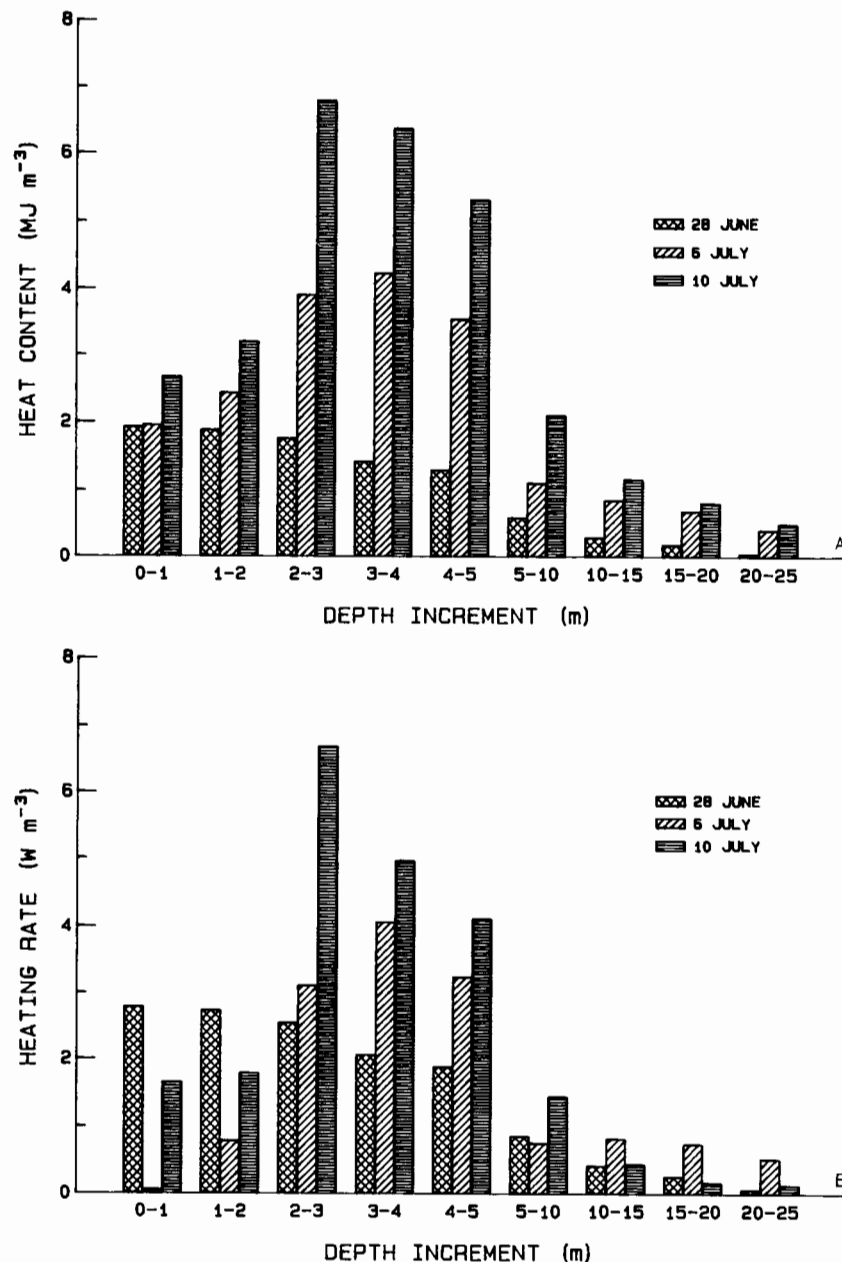


Fig. 6. Observed changes in (a) heat content and (b) heating rates in the water column beneath the Mould Bay lead.

of $F(z, t)$ which must take into account not only light transmitted through the bottom of the lead but also light entering the ocean through the ice (see Figure 8). To calculate downwelling irradiance at the bottom of the ice (F_{ri}), we employed a two-stream, multilayer radiative transfer model [Perovich, 1990] driven by observed changes in ice thickness, surface conditions, and the magnitude of F_r . The spectral distribution of F_r (which also affects the fraction of F_r transmitted by the ice) was estimated using cloud cover values (C) shown in Table 1 and observational data on the relationship between C and $F_r(\lambda)$ taken from Grenfell and Perovich [1984]. Results of these calculations are given in Table 1. To determine the attenuation of F_r below the ice, we need to know the optical properties of the water column. Unfortunately, these properties appear to have undergone substantial changes during the experimental period. The observations (Figure 6b) indicate strong extinction coefficients

increases in the halocline between June 28 and July 10, and we suspect that the stable density stratification below this would also lead to vertical gradients in algae concentration and corresponding gradients in the extinction coefficients. Lacking any specific information on such variations, we decided to examine two extreme cases which are likely to bracket the Mould Bay conditions: (1) very clear Arctic water and (2) relatively opaque water. Extinction coefficients for the Arctic water were obtained from Smith [1973] and Grenfell [1979], while values reported for "dirty" Gulf of California water [Neumann and Pierson, 1966] were used for the opaque case.

Because most of the energy contained in F_{ri} lies in the 450- to 600-nm band where the extinction coefficients are relatively constant with wavelength, absorption of F_{ri} in the water can be approximated with a single extinction coefficient. This is not the case for radiation transmitted through

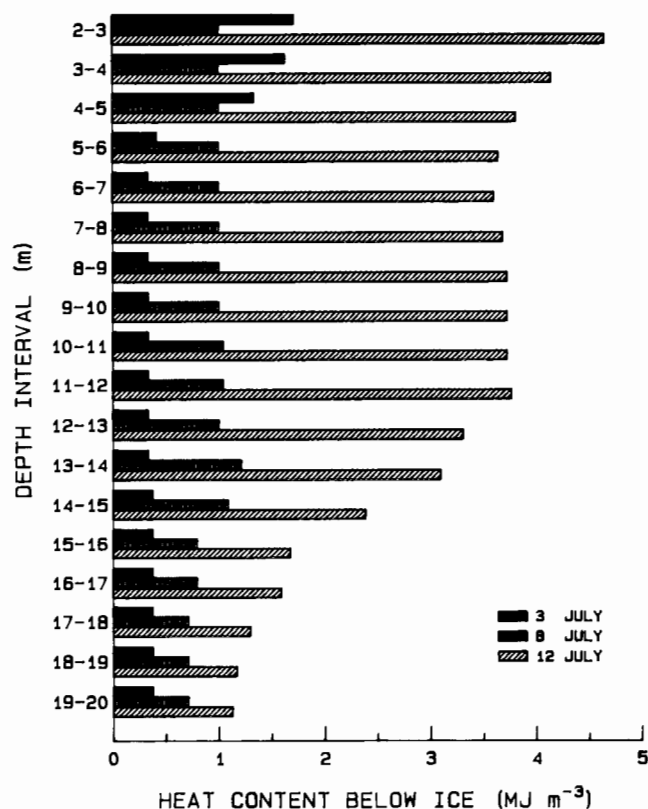


Fig. 7. Observed changes in upper ocean heat content beneath dynamically active ice north of Prince Patrick Island.

the lead (F_{rw}), however, where attenuation of near-infrared energy is much less rapid than in the ice. To estimate the rate at which this energy was absorbed, we first calculated $F_{rw}(z, \lambda)$ using Beer's Law and spectral extinction coefficients spaced at 10-nm intervals between 400 and 1000 nm, again assuming that the spectral distribution of F_r was similar to that found by Grenfell and Perovich [1984]. Results were then integrated over wavelength to obtain $F_{rw}(z)$. To simplify the subsequent model calculations, we then defined i_w to be the fraction of F_r absorbed in a layer of thickness Δz at a depth z , i.e., $i_w = \{F_{rw}(z - 0.5\Delta z) -$

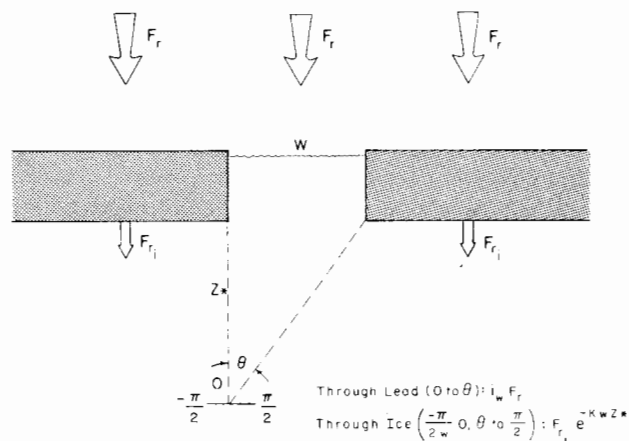


Fig. 8. Schematic illustrating the treatment of shortwave radiation in the water beneath the ice-lead system.

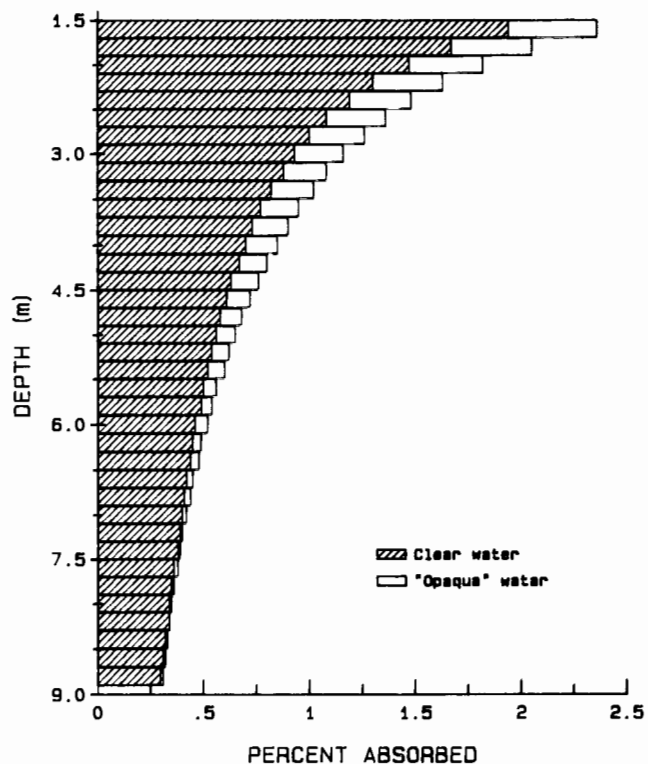


Fig. 9. Depth-dependent decrease in the percent of incoming shortwave radiation absorbed by the two water types under cloudy skies. Each bar represents one of the 0.20-m-thick layers used in the model calculations.

$F_{rw}(z + 0.5\Delta z)/F_r$. In general, i_w will be a function of cloudiness and water type. Figure 9 shows calculated values of $i_w(z)$ for clear Arctic water and "opaque" water under cloudy skies, assuming a depth increment of 0.2 m. Note that below a depth of about 8 m there is slightly less energy absorbed by the opaque water than by the clear water. This is a result of the greater energy depletion in upper part of the water column.

The contributions made by F_{ri} and F_{rw} to $F(z, t)$ depend on the depth and the location relative to the lead. Let us first consider energy absorbed beneath the edge of the lead where the field observations were made. We shall assume that F_{ri} and F_{rw} are both diffuse and that we may neglect limb darkening. This latter assumption is reasonable when there is substantial scattering in the water but will tend to slightly overestimate the influence of F_{rw} when the water is clear. As can be seen from Figure 8, the amount of radiation reaching a depth z depends on the solid angles subtended by the lead and by the ice on either side of the lead. In the two-dimensional case of an infinitely long lead we may write

$$\begin{aligned} \Delta F(z, t) = & \frac{1}{2} \int_0^{\theta_1} i_w F_r(t) \cos \theta d\theta \\ & + \frac{1}{2} \int_{-\pi/2}^0 F_{ri}(t) \exp(-k_w z_*) \cos \theta d\theta \\ & + \frac{1}{2} \int_{\theta_1}^{\pi/2} F_{ri}(t) \exp(-k_w z_*) \cos \theta d\theta \end{aligned} \quad (3)$$

where $\theta_1 = \tan^{-1}(W/z_*)$ is the angle subtended by the lead, W is the width of the lead, $z_* = z - 0.9H$ is the depth below the bottom of the ice, and k_w is an effective extinction coefficient describing attenuation of F_{ri} by the water; values used for k_w were 0.05 m^{-1} when the water was clear and 0.16 m^{-1} when it was opaque. If $z_* \leq 0$, then $\theta_1 = 0$ and F_{ri} does not contribute to $\Delta F(z, t)$. If we define

$$L(z) = \frac{1}{2} \int_0^{\theta_1} \cos \theta \, d\theta \quad (4)$$

we may rewrite (3) as

$$\Delta F(z, t) = L(z)i_w F_r(t) + [1 - L(z)]\Delta F_{ri}(t) \quad (5)$$

where $\Delta F_{ri} = F_{ri}[\exp[-k_w(z - \Delta z/2)] - \exp[-k_w(z + \Delta z/2)]]$. Equation (5) can easily be modified to estimate radiation input at other locations in the vicinity of the lead by changing the limits of integration in L .

June 28 to July 10 Simulations

Equation (1) was integrated with respect to time using the initial temperature profile of June 28, observed boundary temperatures at 1.5 and 9.1 m, and values of $\Delta F(z, t)$ calculated from (5). Predicted temperature profiles for the clear and opaque water on July 10 are compared with observations in Figure 10. Not only are the magnitude and location of the predicted temperature maxima in reasonable agreement with the measurements, but the general shapes of the theoretical and observed profiles are also quite similar. This demonstrates that the thermal structure was in fact controlled by the input of shortwave radiation and that vertical heat transport beneath the halocline was largely the result of diffusive processes. Although the predicted temperature maximum in the opaque water is almost exactly the same as that which was observed, actual temperatures below about 2.5 m are slightly colder than would be expected even in very clear water. In the clean water case the total input of shortwave radiation to the layer during the period was 33.3 MJ/m^2 , of which 1.7 MJ/m^2 was conducted upward to the mixed layer and 0.2 MJ/m^2 to the deeper water. The observed heat content in the water column was 28 MJ/m^2 , about 3 MJ/m^2 less than that calculated for the clean water and 11 MJ/m^2 less than that for the opaque water. The most likely explanation for this difference is lateral mixing of warm water beneath the lead with cooler water from beneath the ice. A mean horizontal heat flux of $0.5\text{--}2.0 \text{ W/m}^2$ would be needed to bring the calculated curves into agreement with the observed curves.

Vertical variations in the amount of algae could also have contributed to the cooler temperatures. If algal concentrations decreased with depth below the halocline, less energy would be absorbed in the lower part of the layer, and heating would be somewhat smaller than predicted. While we have no direct evidence that this was the case, Figure 6b suggests the presence of an absorption maximum near 2 m between July 6 and July 10; substantial absorption in the 3- to 5-m region is also indicated. We conclude that there was an algae maximum in the vicinity of the halocline by July 10 but that significant amounts of algae also existed below this maximum. In fact, Figure 6 indicates that by July 10, nearly all the shortwave energy was being absorbed in the upper 10 m of the water column. It is quite possible that attenuation

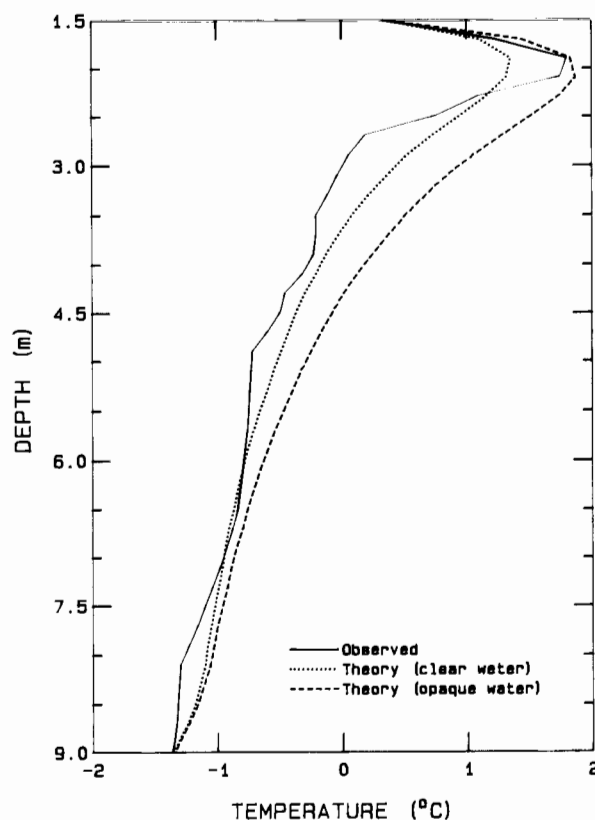


Fig. 10. Comparison of observed and predicted temperature profiles beneath the edge of the lead on July 10.

directly below the halocline was even larger than assumed in the opaque case and that values below about 5 m were somewhat smaller. Nevertheless, cooling produced by horizontal advection is still required to explain the observed temperature profile.

While available evidence suggests that currents and tidal motions beneath the ice were relatively weak, we cannot say precisely how much lateral mixing actually occurred. We can, however, estimate horizontal temperature gradients in the absence of such mixing. Figure 11 shows predicted temperature profiles on July 10 at several locations beneath the ice and lead. The far-field profile was calculated assuming that there was no contribution from F_{ri} , and that the initial temperature profile beneath the ice was at the salinity-determined freezing point of the water. Top and bottom boundary temperatures beneath the ice were fixed at the freezing point of the water, while observed values were used for boundary temperatures beneath the lead. Values of $\Delta F(z, t)$ as a function of distance (x) from the center of the lead were calculated from (4) and (5) after determining appropriate limits of integration (see Figure 8). As expected, the largest horizontal differences occur in the vicinity of the temperature bulge and decrease with increasing distance from the lead. Once x exceeds about 200 m, temperatures are within a few hundredths of a degree of the far-field values.

Although reduced substantially, the temperature maximum was found to exist even in the far-field case, showing that most of the shortwave energy transmitted through the ice would still be trapped in the water column regardless of the existence of nearby leads. The magnitude of the far-field maximum was determined primarily by F_{ri} , not by the

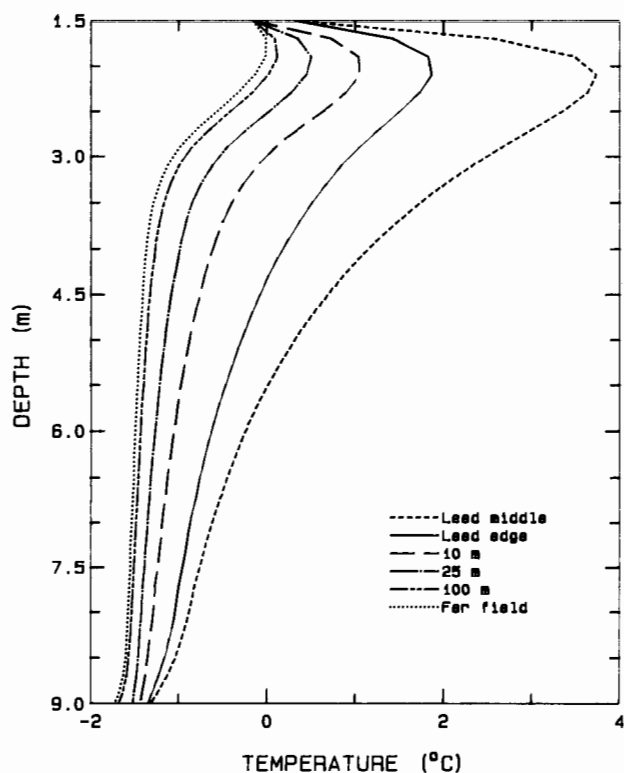


Fig. 11. Predicted horizontal variations in temperature for the opaque water case, assuming no horizontal advection.

proximity of the ice. For example, when F_{ri} was arbitrarily increased by an order of magnitude, the far-field temperature bulge approached 4°C and was similar in shape to that found beneath the center of the lead. Horizontal transport of heat from the lead would of course act to strengthen the bulge beneath the ice.

It should be remembered that the horizontal variations in temperature shown in Figure 11 are the largest that could exist and that the actual gradients must be considerably smaller. Taking into account changes in lead width, we find that the net heat input through the halocline beneath the lead would have been about 715 MJ (per meter of lead length) between June 28 and July 10. Assuming that horizontal gradients beneath the lead were small and that the profiles observed at the edge of the lead were representative of the vertical temperature distribution leads to the conclusion that about 60% of the energy transmitted through the lead was carried beneath the ice. The fact that so much of this energy appears to have remained in the vicinity of the lead suggests that the lateral mixing must have been primarily the result of tidal motions.

July 10 to August 10 Simulations

While the CTD measurements were terminated on July 10, it is known that the ice cover in Mould Bay was present throughout the remainder of the summer (S. Digby, personal communication, 1988). Thinning of the ice and continued widening of the lead would cause the energy input to the water column to remain large in spite of decreases in F_r . To obtain at least a crude estimate of the probable warming during this period, we carried out another series of simulations driven largely by observations of F_r made at the Mould

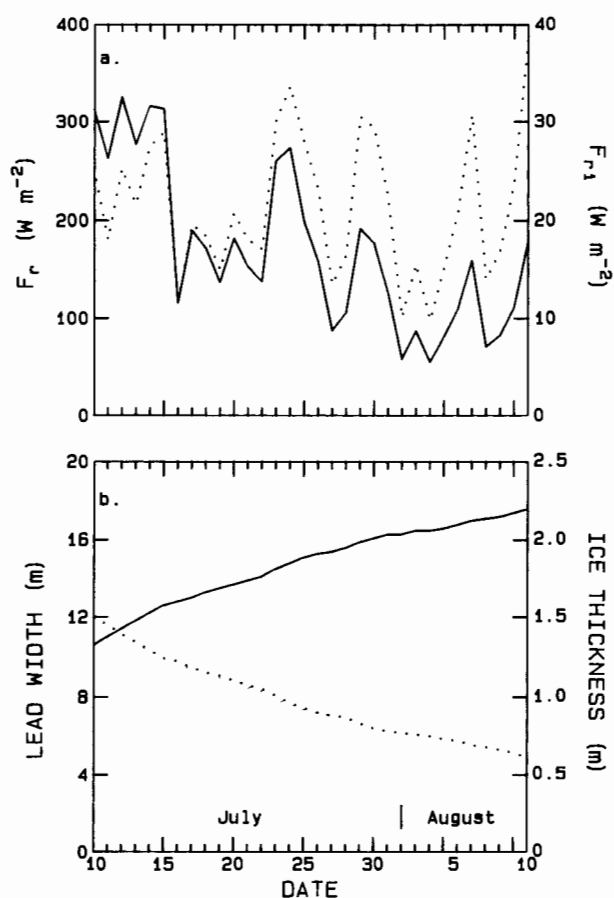


Fig. 12. Forcing used to model water temperature changes between July 10 and August 10: (a) incident shortwave radiation (solid curve) observed at the Mould Bay Weather Station and calculated energy transmission through the ice, F_{ri} (dotted curve), and (b) estimated lead width (solid curve) and ice thickness (dotted curve).

Bay Weather Station (Figure 12a). To estimate $H(t)$ and $W(t)$, we correlated changes in ice thickness and lead width with F_r between June 28 and July 10 and then used these results in conjunction with the values of F_r shown in Figure 12a to obtain daily values of ΔH and ΔW . Results of these calculations are shown in Figure 12b and appear to be quite reasonable. With the estimated $H(t)$ and the observations of $F_r(t)$ and cloudiness we were then able to calculate F_{ri} (Figure 12a) as before. Since the surface layer was well mixed and in contact with the heat sink of the ice, we assumed that there was no appreciable heat buildup in the surface layer and thus that the temperature at the upper boundary ($z = 1.5$ m) remained constant throughout the period. The lower boundary ($z = 9.1$ m) temperature was allowed to increase at a rate similar to that observed during the June 28 to July 10 period. It can be seen that thinning does cause F_{ri} to increase somewhat even though there is a substantial drop in incident shortwave radiation at the surface. Widening of the lead, however, was not rapid enough to prevent slight decreases in the amount of energy entering the ocean through the lead after the middle of July.

Figure 13 shows the predicted evolution of the temperature profile beneath the edge of the lead, assuming cloudy skies and opaque water. The heat content below 1.5 m increased from 39 MJ/m² on July 10 to 104 MJ/m² on August

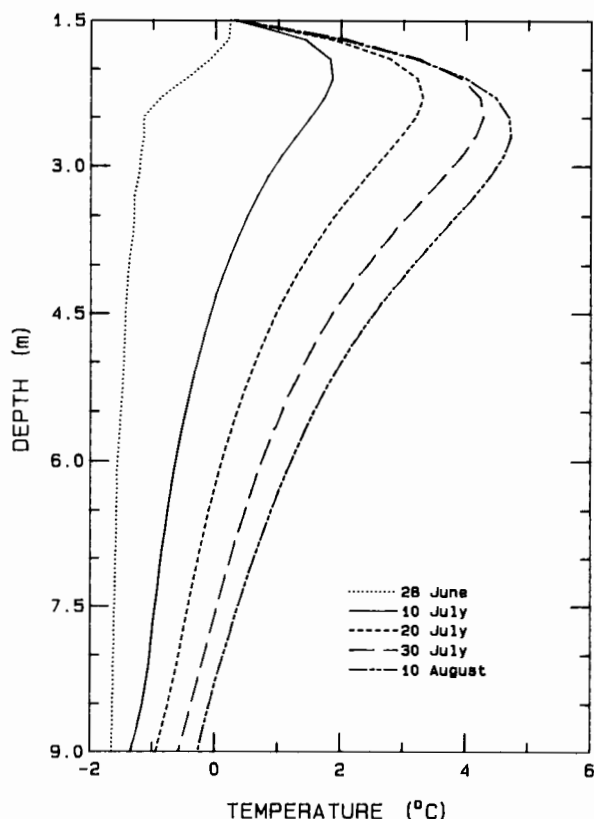


Fig. 13. Time series of predicted temperature profiles in opaque water beneath the edge of the lead between July 10 and August 10.

10, while the temperature maximum increased by almost 2°C. The rate of increase in both heat content and maximum temperature began to diminish after mid-July. In the case of heat content this was simply the result of the decreasing WF_r , but the effect was compounded for the temperature maximum by increased conductive losses and a vertical expansion of the bulge. Interestingly, the model also predicts a downward migration of the bulge with time. The reason for this was the steeper temperature gradient above the bulge which caused more heat to be conducted upward than downward. The far-field temperature maximum beneath the ice became quite well developed during this period, reaching about 2°C above the freezing point, and also moving downward with time. The amount of heat contained in the water column by August 10 would be sufficient to melt 40–50 cm of ice (depending on the brine volume) in the vicinity of the lead and about one third this amount in the far field. Some additional heat was undoubtedly added during the remainder of the month, but this would be unlikely to increase the total heat content by more than 5–10%.

It is of interest to examine at what point continued solar heating would have a destabilizing effect on the salinity-induced pycnocline. To address this issue, we performed a series of calculations using the density equation of Gebhart and Mollendorf [1977] and the measured salinity profile of July 10. The results indicate that water temperatures would need to exceed about 20°C before there could be any chance of instability and, considering the temperature profile expected for solar heating, this figure could be substantially larger. It is unlikely then that thermally induced density

changes in the polar oceans would ever be sufficient to produce a breakdown of such a pycnocline.

CONCLUSIONS

Substantial amounts of solar energy enter the polar oceans, both through the ice and through leads. In regions where the ice is dynamically active, much of this energy contributes directly to melting of the ice cover, at rates which depend on the relative ice-water velocity and on the characteristics of the laminar sublayer adjacent to the melting ice [McPhee *et al.*, 1987]. In bays, fjords, and some coastal regions where the ice remains relatively static and there is limited ocean circulation, surface meltwater from the ice and nearby land tends to become stratified and produces, in effect, a solar pond that traps most of the shortwave radiation absorbed below the pycnocline. If the ice remains throughout the summer, the trapped heat will be slowly released during the fall as the ice grows and rejected brine causes entrainment of the warmer water. The net effect will be to reduce the amount of fall growth, resulting in a somewhat thinner ice cover than would otherwise be the case. Usually, however, the ice will at some point begin to break up and become mobile. Subsequent mechanical mixing then destroys the pycnocline and underlying thermal structure, producing a situation analogous to that in the active ice zone. Release of the trapped heat tends to accelerate the decay cycle by thinning of the ice and by lateral erosion from the floe edges. Nevertheless, the mechanism of primary importance in the final disappearance of a seasonal ice cover remains the positive feedback between decreasing ice concentration and increasing solar input to the water. The significance of the salinity stratification in this process is related directly to the ice thickness and the fractional lead area present while the ice was immobile.

Conditions encountered at Mould Bay, namely an isolated lead with weak tidal currents perpendicular to the axis of the lead, were ideal for studying the interaction of F_r with the ice and underlying water. Despite the lack of information on horizontal variations in the temperature and structure of the water column, sufficient data were available to give us at least a general picture of what happened beneath the lead. The theoretical calculations establish that the temperature maximum was caused by solar heating and indicate that a small maximum should have developed everywhere beneath the ice by July 10, regardless of whether leads were present or not. Probably the least understood aspect of the observed changes was how the vigorous biological activity in the water affected the vertical distribution of transmitted shortwave energy. Once bottom melting begins, organisms attached to the underside of the ice quickly drop off, and primary production is largely limited to the water column. There is some evidence to suggest that the thermally induced density stratification below the pycnocline and the exponentially decreasing light levels may have combined to produce vertical gradients in algae concentration. If this was the case, then positive feedback between algae growth and water temperature is likely to have occurred near the pycnocline. Relatively little attention has been paid to regional effects of leads and meltwater on biological activity in the upper part of the water column, but it is clearly a subject that merits further study.

Acknowledgments. The authors would like to thank F. Carsey, S. Digby-Argus, and B. Holt for their gracious assistance in the field program. We would also like to express our appreciation to T. C. Grenfell for his helpful suggestions and contributions to the field program. This research was made possible by support from the Office of Naval Research, Arctic Program, under contracts N00014-90-J-1075 and N000014-89-WM-24004.

REFERENCES

- Aagaard, K. L., L. K. Coachman, and E. Carmack, On the halocline of the Arctic Ocean, *Deep Sea Res.*, 28, 529-545, 1981.
- Andreas, E. L., and S. F. Ackley, On the differences in ablation seasons of Arctic and Antarctic sea ice, *J. Atmos. Sci.*, 39, 440-447, 1982.
- Buzuyev, A. Ya., and K. N. Fedorov, On the similarity of thermal patterns in fractures among Arctic ice and freshwater lakes (in Russian), *Probl. Arct. Antarct.*, 41, 99-101, 1973.
- Cox, G. F. N., Thermal expansion of sea ice, *J. Glaciol.*, 29, 425-432, 1983.
- Culkin, F., and N. D. Smith, Determination of the concentration of potassium chloride solution having the same electrical conductivity, at 15°C and infinite frequency, as standard seawater of salinity 35‰ (chlorinity 19‰), *IEEE J. Oceanic Eng.*, OE-5(1), 22-23, 1980.
- Doronin, Yu. P., and D. E. Kheisin, *Sea Ice*, 323 pp., Amerind, New Delhi, 1977.
- Gebhart, B., and J. C. Mollendorf, A new density relation for pure and saline water, *Deep Sea Res.*, 24, 831-848, 1977.
- Gordon, A. L., Seasonality of southern ocean sea ice, *J. Geophys. Res.*, 86, 4193-4197, 1981.
- Grenfell, T. C., The effects of ice thickness on the exchange of solar radiation over the polar oceans, *J. Glaciol.*, 22, 305-320, 1979.
- Grenfell, T. C., A theoretical model of the optical properties of sea ice in the visible and near infrared, *J. Geophys. Res.*, 88, 9723-9735, 1983.
- Grenfell, T. C., and G. A. Maykut, The optical properties of ice and snow in the Arctic Basin, *J. Glaciol.*, 18, 445-463, 1977.
- Grenfell, T. C., and D. K. Perovich, Spectral albedos of sea ice and incident solar irradiance in the southern Beaufort Sea, *J. Geophys. Res.*, 89, 3573-3580, 1984.
- Hoare, R. A., Problems of heat transfer in Lake Vanda, a density stratified Antarctic lake, *Nature*, 210, 787-789, 1966.
- Hoare, R. A., K. B. Popplewell, D. A. House, R. A. Henderson, W. M. Prebble, and A. T. Wilson, Lake Bonney, Taylor Valley, Antarctica: A natural solar energy trap, *Nature*, 202, 866-888, 1964.
- Holt, B., and S. A. Digby, Processes and imagery on fast first-year sea ice during the melt season, *J. Geophys. Res.*, 90, 5045-5062, 1985.
- Hutchinson, G. E., *A Treatise on Limnology*, vol. 1, *Geophysics, Physics and Chemistry*, 1015 pp., John Wiley, New York, 1957.
- Langleben, M. P., On the factors affecting the rate of ablation of sea ice, *Can. J. Earth Sci.*, 3, 431-439, 1966.
- Langleben, M. P., The decay of an annual cover of sea ice, *J. Glaciol.*, 11, 337-344, 1972.
- Lewis, E. L., The practical salinity scale 1978 and its antecedents, *IEEE J. Oceanic Eng.*, OE-5(1), 3-8, 1980.
- Maykut, G. A., Large-scale heat exchange and ice production in the central Arctic, *J. Geophys. Res.*, 87, 7971-7985, 1982.
- Maykut, G. A., and T. C. Grenfell, The spectral distribution of light beneath first-year sea ice in the Arctic Ocean, *Limnol. Oceanogr.*, 20, 554-563, 1975.
- Maykut, G. A., and D. K. Perovich, The role of shortwave radiation in the summer decay of a sea ice cover, *J. Geophys. Res.*, 92, 7032-7044, 1987.
- Maykut, G. A., and N. Untersteiner, Some results from a time dependent, thermodynamic model of sea ice, *J. Geophys. Res.*, 76, 1550-1575, 1971.
- McPhee, M. G., G. A. Maykut, and J. H. Morison, Dynamics and thermodynamics of the ice/upper ocean system in the marginal ice zone of the Greenland Sea, *J. Geophys. Res.*, 92, 7017-7031, 1987.
- Neumann, G., and W. J. Pierson, *Principles of Physical Oceanography*, 545 pp., Prentice-Hall, Englewood Cliffs, N. J., 1966.
- Perovich, D. K., On the summer decay of a sea ice cover, Ph.D. dissertation, 176 pp., Geophys. Program, Univ. of Wash., Seattle, 1983.
- Perovich, D. K., Theoretical estimates of light reflection and transmission by spatially complex and temporally varying sea ice covers, *J. Geophys. Res.*, 90, 9557-9567, 1990.
- Perovich, D. K., and T. C. Grenfell, Laboratory studies of the optical properties of young sea ice, *J. Glaciol.*, 27, 331-346, 1981.
- Smith, R. C., Optical properties of the Arctic upper water, *Arctic*, 26, 303-313, 1973.
- Untersteiner, N., On the mass and heat budget of Arctic sea ice, *Arch. Meteorol. Geophys. Bioklimatol., Ser. A*, 12(2), 151-182, 1961.
- Wiegand, R. C., and E. C. Carmack, A wintertime temperature inversion in Kootenay Lake, British Columbia, *J. Geophys. Res.*, 86, 2024-2034, 1981.
- Zubov, N. N., *Arctic Ice* (in Russian), 491 pp., Glavsevmorputi, Moscow, 1945. (English translation, U.S. Oceanographic Office, Suitland, Md., 1965.)
- G. A. Maykut, Department of Atmospheric Sciences, AK-40, University of Washington, Seattle, WA 98195.
- D. K. Perovich, U.S. Army Cold Regions Research and Engineering Laboratory, 72 Lyme Road, Hanover, NH 03755.

(Received January 16, 1990;
revised March 23, 1990;
accepted March 30, 1990.)